Fault-Tolerant Optimization Control of Open-Winding Dual Three-Phase PMSM Drives in Full Operation Range

Linlin Lu, *Student Member, IEEE*, Xueqing Wang, *Senior Member, IEEE*, Luhan Jin, *Student Member, IEEE*, Yao Mao, *Member, IEEE*, Qiliang Bao, *Member, IEEE*, and Zheng Wang, *Senior Member, IEEE*

***Abstract*—Open-winding dual three-phase permanent-magnet synchronous motor (DTP-PMSM) has high fault-tolerant capability because of its sufficient control degrees of freedom. This article proposes an optimization control scheme to explore the fault-tolerant capability of open-winding DTP-PMSM drives with open-phase fault in full operation range. First, the relationships between the operation states and minimum-copper-loss (ML) fault-tolerant mode and maximum-torque (MT) fault-tolerant mode are analyzed in detail. Three optimization problems are then formulated based on the objectives for each operation state, which can be effectively solved by utilizing the interior point method. Compared to the existing MT and ML schemes, the proposed scheme can achieve the theoretical highest torque output capability and lowest copper loss in full operation range. Comprehensive experimental results are presented to substantiate the effectiveness and superiority of the proposed fault-tolerant optimization control scheme.**

***Index Terms*—Fault-tolerant control, full operation range, open-phase fault, open-winding dual three-phase permanent-magnet synchronous motor (DTP-PMSM).**

I. Introduction

THE reliability of motor drives is critical in many applications such as electric vehicles and aerospace. The dual three-phase permanent-magnet synchronous motor (DTP-PMSM) is characterized by its excellent fault-tolerant performance, which can continue to operate after faults due to its multiple windings [1], [2], [3]. Thus, the research on fault-tolerant control of DTP-PMSM drives is a hot topic. Besides, additional degrees of freedom can be exploited by changing the winding configurations. Open-winding PMSM breaks the neutral points and is fed by two inverters at both ends. This configuration has higher control dimensions [4], [5]. By combining the advantages of multiple phase and open winding, open-winding DTP-PMSM can obtain better fault-tolerant performance.

Among different types of faults in motor drives, the open-phase fault is common [6], [7]. Under the open-phase fault, the current in the faulty phase of DTP-PMSM drive will be forced to zero. As a result, the faulty currents can hardly follow their references effectively and obvious current distortion will occur, leading to torque ripple or even unstable operation [3], [8], [9], [10], [11]. The simplest fault-tolerant solution for open-phase fault in DTP-PMSM drive is to remove the whole faulty winding set. Although this strategy can suppress the torque ripple, the advantages of multiple windings can hardly be fully utilized. Thus, optimizing the fault-tolerant currents for open-phase faults has been widely studied.

The basic goal of fault-tolerant control in open-phase fault for dual three-phase PMSM drives is to reduce torque ripple. The minimum copper loss and the maximum torque output are two major optimization objectives of fault-tolerant control [12]. The minimum-copper-loss (ML) strategy aims to minimize the total copper loss, while the maximum-torque (MT) strategy minimizes the maximum phase copper loss for the given torque [13], [14]. In terms of ML strategies, Che et al. [15] considers the sinusoidal phase currents and derives the current references for six-phase induction motor drives with both isolated and connected neutral points, respectively. On this basis, Wang et al. [16] remove unnecessary constraints and obtains the theoretical ML current references for DTP-PMSM drives.

As for MT strategies for DTP-PMSM drives under open-phase faults, Wang et al. [17] injected the second harmonics into the current references to improve the MT optimization objective. Feng et al. [18] derived a computation-efficient fault-tolerant MT scheme for interior PMSM by injecting harmonic components according to the changing machine parameters. In [19], the torque output capability is further improved by optimizing the current references without using the constraint of sinusoidal phase currents.

Previous studies on ML and MT schemes are mostly applied in a single operation state. To achieve the full potential of motor drive system, the characteristics of different operation states should be considered. In [20], a minimum-loss fault-tolerant

Received 25 April 2024; revised 26 August 2024; accepted 9 October 2024. Date of publication 21 October 2024; date of current version 18 December 2024. This work was supported in part by the National Natural Science Foundation of China under Grant 62303333, in part by Sichuan Science and Technology Program 2024JDRC0056, and in part by Sichuan Science and Technology Program of China under Grant 2024NSFSC1492. Recommended for publication by Associate Editor S. C. Yang. *(Corresponding authors: Xueqing Wang; Yao Mao.)*

Linlin Lu, Luhan Jin, Yao Mao, and Qiliang Bao are with the National Key Laboratory of Optical Field Manipulation Science and Technology, Chinese Academy of Sciences, Chengdu 610209, China, also with the Key Laboratory of Optical Engineering, Chinese Academy of Sciences, Chengdu 610209, China, also with the Institute of Optics and Electronics, Chinese Academy of Sciences, Chengdu 610209, China, and also with the University of Chinese Academy of Sciences, Beijing 101408, China (e-mail: lulinlin21@mails.ucas.ac.cn; jinluhan21@mails.ucas.ac.cn; maoyao@ioe.ac.cn; baoqiliang@ioe.ac.cn).

Xueqing Wang is with the College of Electrical Engineering, Sichuan University, Chengdu 610065, China (e-mail: xwang@scu.edu.cn).

Zheng Wang is with the School of Electrical Engineering, Southeast University, Nanjing 210096, China (e-mail: zwang@eee.hku.hk).

Color versions of one or more figures in this article are available at https://doi.org/10.1109/TPEL.2024.3484584.

Digital Object Identifier 10.1109/TPEL.2024.3484584

strategy using global search algorithm is proposed with maximum efficiency for multiphase PMSM drives in whole torque operation range. Sun et al. [21] proposed an online optimization scheme using ML redistribution that can calculate the current references for different faulty phases of symmetrical multiphase machines in full torque operation range. Hu et al. [22] analyze and relate the ML, MT and single three-phase mode control through a coefficient that can switch different modes smoothly for DTP-PMSM drives.

In the above research, ML and MT strategies for multiphase machines with isolated neutral points and connected neutral points have been deeply studied. However, these fault-tolerant schemes are limited by the constraints of zero-sequence subspace or sinusoidal current patterns, which restricts the optimization solution space and hinders the full optimization of copper loss and torque output capability. In addition, the existing researches usually ignore the critical impact of operating frequency on the temperature swing in low-frequency and static operations (LFSOs). To solve these problems, this article proposes a fault-tolerant control scheme that fully utilizes the original optimization solution space of open-winding DTP-PMSM drive in full operation range. By removing the unnecessary constraints of zero-sequence currents (ZSCs) and current patterns, the proposed scheme can optimize the current references from the complete solution space, contributing to reduced copper loss and enhanced torque output capability. To ensure comprehensive optimization in full operation range, the proposed fault-tolerant control scheme considers different operation states, including high-torque operations (HTO), medium-torque and low-torque operations (MLTOs), medium-frequency and high-frequency operations (MHFOs), LFSO.

This rest of this article is organized as follows. Section II describes the machine model and control framework for open-winding DTP-PMSM drives. In Section III, the analysis of fault-tolerant control in full operation range is carried out, and the corresponding optimization objectives are proposed to adapt the different operation states. In Section IV, the ML optimization problem is formulated and solved to obtain the optimal current references, and its performance is compared with other ML schemes. In Section V, the MT optimization problems for MHFO and LFSO are formulated and solved, and their performances are compared with other MT schemes. In Section VI, experiments are carried out to verify the effectiveness and superiority of the proposed control scheme. Finally, Section VII conclude this article.

II. Machine Model and Control

A. Modeling of DTP-PMSM

The open-winding DTP-PMSM drive is shown in Fig. 1. DTP-PMSM has two sets of three-phase windings, phase-ABC and Phase-DEF, which have a $\pi/6$ phase shift. The open-winding topology breaks the neutral point connection and both winding ends are powered by inverters with common dc bus, respectively. INV-1 and INV-2 are two voltage source inverters on both sides of the open-winding DTP-PMSM.

Open-winding DTP-PMSM is a complex nonlinear high-order system. The vector space decomposition (VSD) method is commonly used to transform the machine model into three two-dimensional orthogonal subspaces: α–β; x–y; and o_1–o_2 [23]. The decomposition matrix for open-winding DTP-PMSM

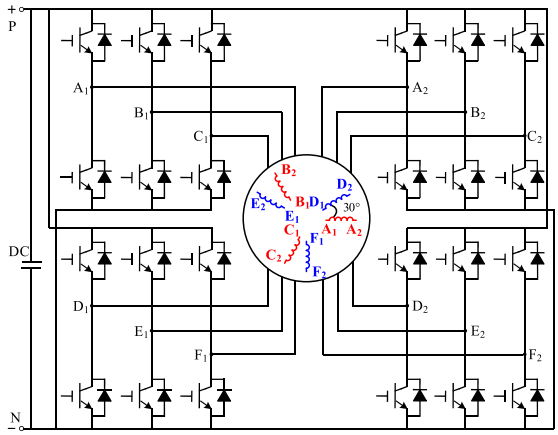

Fig. 1. Open-winding DTP-PMSM drives.

is expressed as

$$[\boldsymbol{T}_{\mathrm{VSD}}] = \begin{bmatrix} \alpha \\ \beta \\ x \\ y \\ o_1 \\ o_2 \end{bmatrix} = \frac{1}{6}\begin{bmatrix} 2 & -1 & -1 & \sqrt{3} & -\sqrt{3} & 0 \\ 0 & \sqrt{3} & -\sqrt{3} & 1 & 1 & -2 \\ 2 & -1 & -1 & -\sqrt{3} & \sqrt{3} & 0 \\ 0 & -\sqrt{3} & \sqrt{3} & 1 & 1 & -2 \\ 2 & 2 & 2 & 0 & 0 & 0 \\ 0 & 0 & 0 & 2 & 2 & 2 \end{bmatrix}. \quad (1)$$

The model can be further simplified by transforming the α–β subspace to d–q subspace, in which the rotating transformation is expressed as

$$[\boldsymbol{T}_{s/r}] = \begin{bmatrix} \cos\theta_e & \sin\theta_e & \mathbf{0}_4 \\ -\sin\theta_e & \cos\theta_e & \mathbf{0}_4 \\ \mathbf{0}_4 & \mathbf{0}_4 & \mathbf{I}_{4\times 4} \end{bmatrix} \quad (2)$$

where θ_e is the electric angle. According to the VSD matrix in (1) and the rotation matrix in (2), the voltage and torque equations of open-winding DTP-PMSM can be obtained as

$$\begin{cases} u_d = R_s i_d + L_d di_d/dt - \omega_r L_q i_q \\ u_q = R_s i_q + L_q di_q/dt + \omega_r L_d i_d + \omega_r \psi_f \\ u_x = R_s i_x + L_{ls} di_x/dt \\ u_y = R_s i_y + L_{ls} di_y/dt \\ u_{o1} = R_s i_{o1} + L_{ls} di_{o1}/dt \\ u_{o2} = R_s i_{o2} + L_{ls} di_{o2}/dt \end{cases} \quad (3)$$

$$T_e = 3n_p\left(\psi_f i_q + (L_d - L_q) i_d i_q\right) \quad (4)$$

where R_s is the stator resistance. L_d, L_q, and L_{ls} are the d-axis, q-axis, and leakage inductances. ω_r is the rotor angular velocity. ψ_f is the amplitude of rotor flux and n_p is the pole pair number.

B. Control Framework

Open-winding DTP-PMSM can share the same control framework with DTP-PMSM using isolated or connected neutral points. The difference lies in the control of ZSCs. There are two zero-sequence paths in the open-winding DTP-PMSM drive supplied by the common dc bus, where the two ZSCs are independent. The ZSCs should be suppressed to zero in healthy operation and track their fault-tolerant references in fault-tolerant operation. According to the voltage equations of open-winding

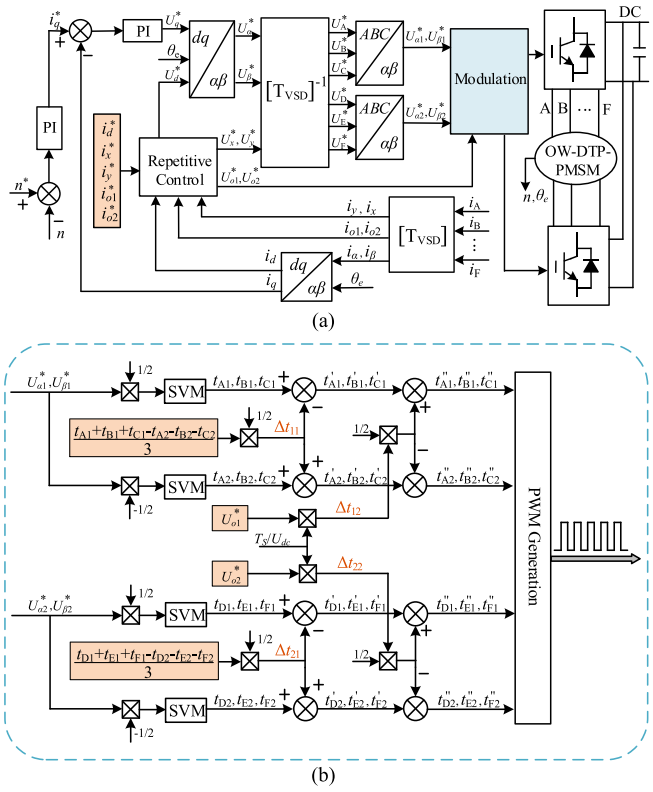

Fig. 2. Control diagram of open-winding DTP-PMSM. (a) Control framework. (b) Modulation framework.

DTP-PMSM in (3), the ZSCs are positively related to their respective zero-sequence voltages (ZSVs). Therefore, the ZSCs can be controlled by introducing the closed-loop current controllers on o_1–o_2 subspace like other subspaces. Fig. 2(a) shows the designed unified vector control framework which is suitable for both normal and fault-tolerant operations. Different operation states can be switched by simply changing the current references. For q-axis, the typical PI control is adopted to achieve the precise closed-loop control for torque. For d-axis, x–y subspace and o_1–o_2 subspace, the repetitive controller is used to track the current references containing ac components precisely. Fig. 2(b) illustrates the modulation framework of open-winding DTP-PMSM drive. The voltage references are divided equally for the inverters at both winding ends. Four identical space vector modulations (SVMs) are utilized to calculate the high-level duration time t_X for each inverter leg. To modulate the ZSVs generated by SVMs as zero, the duration times of zero vector Δt_{11} and Δt_{21} are calculated for phase-ABC and phase-DEF, respectively. On this basis, the duration times of high-level zero vectors Δt_{12} and Δt_{22} should be adjusted to fulfill the tracking of ZSV references from the current controllers on o_1–o_2 subspace. After updating the duration times of zero vectors through the above two steps, the new high-level duration times of each phase t_X'' can be obtained, enabling precise ZSC tracking.

III. Analysis of Fault-Tolerant Control in Full Operation Range

The motor drives should possess the ability to work in full torque and frequency operation ranges, especially in the circumstance of faulty operations. Phase currents will be increased and unequal under open-phase faults, which will degrade the performance of motor drives. Thus, it is necessary to analyze the characteristics of different operating frequencies and operating torques to achieve better fault-tolerant performance.

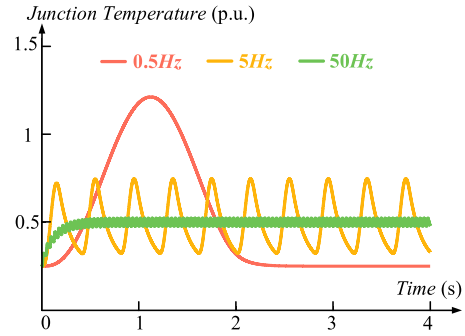

Fig. 3. Junction temperature swing at different frequencies.

A. Analysis of Different Operating Torque

The torque operation range can be divided into MLTO and HTO. Different control strategies should be adopted for different operating torque.

In MLTO, all phase currents are below the current limitation and no overheating problem exists. The total copper loss, one of the fundamental indexes for efficiency, should be considered. Therefore, the ML strategy should be adopted in MLTO, and its objective is to minimize the total copper loss.

In HTO, the torque output is highly required, and large phase currents may exceed their rated value. In this situation, overheating problems should be prevented from motor damage. Therefore, the MT strategy should be adopted under this circumstance, and its objective is to minimize the maximum phase current amplitude under constant torque.

B. Analysis of Different Operating Frequency

Different operating frequencies can affect the magnitude of temperature swing both in windings and inverters. Taking the temperature swing in inverters as an example, the real-time junction temperatures of power devices can be estimated with the thermal resistances and power losses according to the thermal model [24]. To intuitively show the effect of operating frequency on the temperature swing, the junction temperature swing of inverters at different frequencies is shown in Fig. 3. It can be concluded from Fig. 3 that the temperature swing increases significantly as the frequency decreases, reducing the reliability of motor drives. Thus, the small temperature swing in MHFO can be ignored and the large one in LFSO should be suppressed.

C. Mode Selection of Different Operation States

To ensure the fault-tolerant performance in different operation states, this article proposes the minimum-copper-loss optimization control (MLOC) for MLTO and the maximum-torque optimization control (MTOC) for MHFO and LFSO. The switching rules between these control modes are determined by the operating torque and frequency, as shown in Fig. 4. The switching rule between MTOC and MLOC is established based on the operating torque which is related to the phase currents. Specifically, when

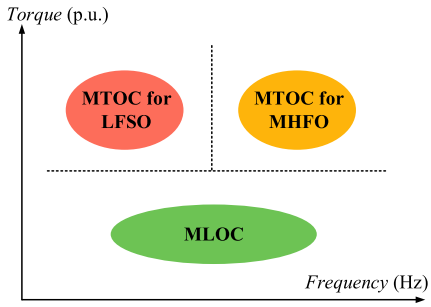

Fig. 4. Mode selection of different torque and frequency operation ranges.

the phase currents are below their rated values, MLOC will be used to improve the operating efficiency by minimizing the total copper loss. Otherwise, MTOC will be adopted to prevent overheating by optimizing the maximum phase copper loss. MTOC is further divided into two modes, and the switching rule between them depends on the temperature swing which is affected by the operating frequency. Since the temperature swing can be negligible in MHFO, the MTOC for MHFO will be applied to reduce the maximum average phase copper loss. Considering the obvious temperature swing in LFSO, MTOC for LFSO will be employed to optimize the maximum instantaneous phase copper loss to suppress the temperature swing.

IV. Minimum-Copper-Loss Optimization Control Scheme

A. Optimization of Current References

MLOC aims to minimize the total copper loss. The instantaneous total copper loss can be calculated in (5) using the power formula with phase currents and stator resistance

$$P_{\mathrm{Cu}} = \left(i_A^2 + i_B^2 + i_C^2 + i_D^2 + i_E^2 + i_F^2\right) R_s. \tag{5}$$

The average total copper loss can be expressed as the integral of instantaneous copper loss in a fundamental period of DTP-PMSM, as shown in

$$\overline{P_{\mathrm{Cu}}} = \frac{1}{2\pi}\int_0^{2\pi} \left(i_A^2 + i_B^2 + i_C^2 + i_D^2 + i_E^2 + i_F^2\right) R_s d\theta_e. \tag{6}$$

By minimizing the instantaneous copper loss at each electric angle, the average total copper loss over a fundamental period is also minimized. Therefore, the instantaneous copper loss in (5) is selected as the objective function for ease of optimization. Since the copper losses are inherently calculated with phase currents, the natural coordinate system is employed to intuitively analyze and formulate the optimization problem.

Apart from the ML objective, the current constraint should also be considered to ensure equivalent torque output before and after fault. According to the torque equation in (4), the torque output is proportional to the q-axis current for surface-mounted PMSMs, while it depends on the d-axis and q-axis currents simultaneously for interior PMSMs. By combining the VSD and rotating transformation, the constraint of phase currents under constant q-axis current can be expressed in (7) for surfaced-mounted PMSMs. For interior PMSMs, the torque constraint should be restructured to meet the corresponding relationship between torque and currents

$$\begin{aligned} & g\left(i_A, i_B, i_C, i_D, i_E, i_F\right) \\ = & -\frac{1}{3}\left(\sin\left(\theta_e\right) i_A + \sin\left(\theta_e - \frac{2}{3}\pi\right) i_B \right. \\ & + \sin\left(\theta_e + \frac{2}{3}\pi\right) i_C + \sin\left(\theta_e - \frac{1}{6}\pi\right) i_D \\ & \left. + \sin\left(\theta_e - \frac{5}{6}\pi\right) i_E + \sin\left(\theta_e + \frac{1}{2}\pi\right) i_F \right) \\ = & \, i_q. \end{aligned} \tag{7}$$

Taking phase-A open-circuit fault as an example, Phase-A current is zero in function g. By combining the objective function of copper loss in (5) and the current constraint in (7), the MLOC optimization problem is formulated in (8), where the phase currents serve as the optimization variables

$$\begin{aligned} & \min P_{\mathrm{Cu}} \\ & \text{s.t. } g\left(0, i_B, i_C, i_D, i_E, i_F\right) = i_q. \end{aligned} \tag{8}$$

The optimization problem in (8) is a convex quadratic problem with linear equality constraints and it can be solved with interior point method [25]. To obtain the current references in the whole fundamental period, the optimization problem is solved with interior point method at each electric angle that is discretized into 200 points. Then, the phase and decoupled current references can be plotted in Fig. 5(a) and (b).

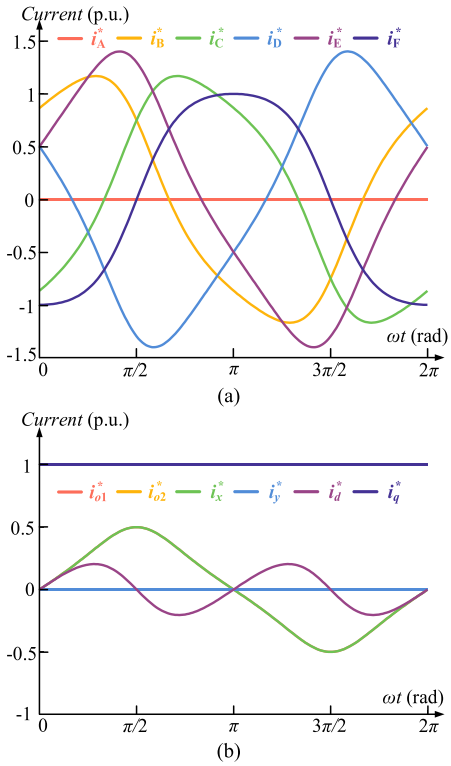

Fig. 5. Current references of the proposed minimum-copper-loss optimization control scheme of open-winding DTP-PMSM drives. (a) Six-phase currents. (b) Currents on d–q, x–y, and o_1–o_2 subspaces.

TABLE I
COMPARISON OF COPPER LOSS AND TORQUE OUTPUT CAPABILITY

Fault-tolerant scheme	Maximum RMS phase current (p.u.)	Maximum peak phase current (p.u.)	Total copper loss (p.u.)	Torque output capability in MHFO	Torque output capability in LSFO
ML Scheme I [28]	1.803	2.55	1.5	55.5%	39.2%
ML Scheme II [17]	1.616	2.628	1.429	61.9%	38.1%
ML Scheme III [16]	1.664	2.628	1.291	60.1%	38.1%
Proposed ML Scheme	1.296	1.983	1.224	77.2%	50.4%

Adopting sinusoidal functions, the currents on d–q, x–y, and o_1–o_2 subspaces can be fitted to expressions as

$$\begin{cases} {i_d}^* = [0.202\sin(2\theta_e) - 0.02\sin(4\theta_e) + 0.002\sin(6\theta_e)]{i_q}^* \\ {i_x}^* = [0.45\sin(\theta_e) - 0.045\sin(3\theta_e) + 0.005\sin(5\theta_e)]{i_q}^* \\ {i_y}^* = 0 \\ {i_{o1}}^* = {i_x}^* \\ {i_{o2}}^* = 0 \end{cases}. \tag{9}$$

Finally, the open-phase fault is tolerated by updating the optimized current references on d–q, x–y, and o_1–o_2 subspaces in Fig. 2(a). It should be noted that the proposed fault-tolerant control scheme is also applicable to open-switch faults which can be considered the special open-phase fault occurring only in half one fundamental period. Therefore, the open-switch faults can be tolerated by directly applying the proposed fault-tolerant control scheme either in the entire fundamental period or only in the faulty half-fundamental period [16], [26].

B. Performance Comparison

To show the superiority of the proposed MLOC scheme, a theoretical comparison is implemented in Table I. For better comparison and understanding, the phase currents and copper losses are given in the form of per unit (p.u.). The torque output capability in MHFO and LFSO can be defined as [19], [27]

$$\eta_{\text{Te\_MHFO}} = \frac{I_{N\_\text{RMS}}}{I_{\text{Max\_RMS}}} \tag{10}$$

$$\eta_{\text{Te\_LFSO}} = \frac{I_{N\_\text{RMS}}}{I_{\text{Max\_peak}}} \tag{11}$$

where I_{N_RMS} is the root-mean-square (RMS) phase currents in healthy operation. $I_{\text{Max\_RMS}}$ is the maximum value of six-phase RMS currents in fault-tolerant operation. $I_{\text{Max\_peak}}$ is the maximum peak phase currents.

Gonzalez-Prieto et al. [28] assume the sinusoidal phase currents and maintains the y-axis current zero, which can reduce the total copper loss to 1.5 p.u. Wang et al. [17] can reduce copper loss to 1.429 p.u. by injecting the second harmonics and limiting d_2-axis current to zero. Wang et al. [16] further optimize the current references by removing any unessential constraints, and the copper loss is reduced to 1.291 p.u. As for the proposed MLOC scheme, the fault-tolerant capability in open-winding PMSM is fully utilized by optimizing the proposed quadratic programming problem. Using the obtained optimal current references, the copper loss can be reduced to the theoretical lowest copper loss of 1.224 p.u. In addition, the torque output capabilities in both MHFO and LSFO are improved compared with the above ML schemes, as given in Table I.

V. MAXIMUM-TORQUE OPTIMIZATION CONTROL SCHEME

A. Medium-Frequency and High-Frequency Operations

At medium and high frequencies, the average phase copper loss during the entire fundamental period should be optimized, and it can be expressed as

$$\overline{P_{\text{Cu\_X}}} = \frac{1}{2\pi}\int_0^{2\pi} i_{\text{X}}^2 R_s d\theta_e. \tag{12}$$

Assuming that Phase-A is in open-circuit fault, the maximum average phase copper loss is regarded as the objective function which can be expressed as

$$\overline{P_{\text{Cu\_Max}}} = \max\left(\overline{P_{\text{Cu\_B}}}, \overline{P_{\text{Cu\_C}}}, \overline{P_{\text{Cu\_D}}}, \overline{P_{\text{Cu\_E}}}, \overline{P_{\text{Cu\_F}}}\right). \tag{13}$$

Since the average phase copper losses in (13) are directly calculated using phase currents, the six-phase currents are adopted as optimization variables to avoid unnecessary coordinate transformation and reduce the optimization complexity. Combining the objective function of maximum average phase copper loss in (13) and the current constraint in (7), the MTOC problem for MHFO can be formulated in (14), and phase currents serve as optimization variables

$$\begin{aligned} &\min \overline{P_{\text{Cu\_Max}}} \\ &\text{s.t. } g\left(0, i_{\text{B}}, i_{\text{C}}, i_{\text{D}}, i_{\text{E}}, i_{\text{F}}\right) = 0. \end{aligned} \tag{14}$$

Considering the complexity of handling the two-level optimization problem using the traditional single-objective methods, the inequality constraints are introduced to simplify the optimization process. By constraining each average phase copper loss $\overline{P_{\text{Cu\_X}}}$ no larger than the maximum average copper loss $\overline{P_{\text{Cu\_Max}}}$, the two-level optimization problem in (14) is transformed to a standard convex quadratic optimization problem in (15) to minimize the value of maximum average copper loss

$$\begin{aligned} &\min \overline{P_{\text{Cu\_Max}}}. \\ &\text{s.t. } \begin{cases} \overline{P_{\text{Cu\_X}}} \le \overline{P_{\text{Cu\_Max}}} \\ g(0, i_{\text{B}}, i_{\text{C}}, i_{\text{D}}, i_{\text{E}}, i_{\text{F}}) = 0 \end{cases} \end{aligned} \tag{15}$$

The electric angle θ_e is discretized by 200 points from 0 to 2π for easy solving, and the average phase copper losses are transformed to the summation of discretized points. Besides, the equality constraint g should be satisfied at all the discretized θ_e in the MTOC problem for MHFO. By applying the interior point method, the optimized phase current references can be plotted in Fig. 6(a), and the corresponding decoupled current references are shown in Fig. 6(b).

Adopting sinusoidal functions, the currents on d–q, x–y, and o_1–o_2 subspaces can be fitted to expressions as

$$\begin{cases} {i_d}^* = [0.25\sin(2\theta_e) - 0.031\sin(4\theta_e) + 0.004\sin(6\theta_e)]{i_q}^* \\ {i_x}^* = [0.4\sin(\theta_e) - 0.05\sin(3\theta_e) + 0.006\sin(5\theta_e)]{i_q}^* \\ {i_y}^* = 0 \\ {i_{o1}}^* = [0.479\sin(\theta_e) - 0.06\sin(3\theta_e) + 0.007\sin(5\theta_e)]{i_q}^* \\ {i_{o2}}^* = [-0.71\cos(\theta_e) + 0.009\cos(3\theta_e) - 0.001\cos(5\theta_e)]{i_q}^* \end{cases}. \tag{16}$$

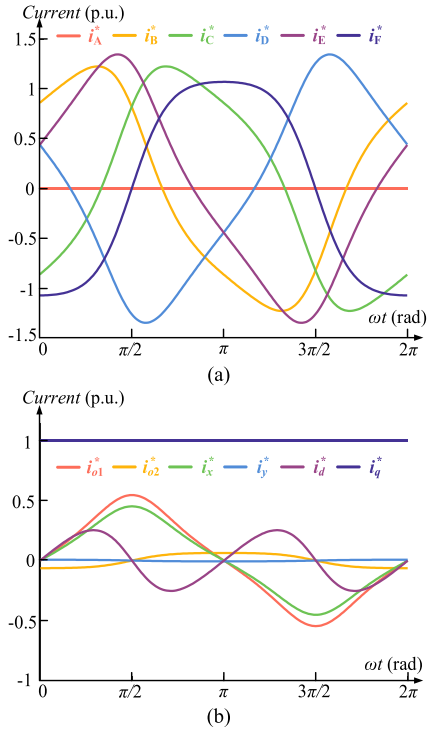

Fig. 6. Current references of the proposed maximum-torque optimization control scheme of open-winding DTP-PMSM drives in MHFO. (a) Six-phase currents. (b) Currents on d–q, x–y , and o_1–o_2 subspaces.

B. Low-Frequency and Static Operations

The temperature swing is influenced by frequency and magnitude of phase currents. The large instantaneous phase currents in LFSO and HTO increase the temperature swing, which can be solved by minimizing instantaneous phase copper loss at any electric angles. Thus, the MTOC optimization problem for LFSO should be formulated using real-time phase currents and copper losses.

To achieve the objective of minimizing the maximum instantaneous phase copper loss, the phase currents should be constrained within an allowable range at any electric angles. At any electric angles, if one phase current is reduced, the rest phase currents should be increased to maintain the current constraint of constant torque output in (7). When all instantaneous phase currents converge to the same value, this value can be adopted as the current limitation I_m at this electric angle. Assuming that phase-A is in open-circuit fault, the function of current limitation is expressed in (17) with the electric angle θ_e as the independent variable.

$$I_m(\theta_e) = \frac{3i_q}{\left(\begin{array}{l}\left|\sin(\theta_e - \frac{2}{3}\pi)\right| + \left|\sin(\theta_e + \frac{2}{3}\pi)\right| + \left|\sin(\theta_e - \frac{1}{6}\pi)\right| \\ + \left|\sin(\theta_e - \frac{5}{6}\pi)\right| + \left|\sin(\theta_e + \frac{1}{2}\pi)\right|\end{array}\right)}. \tag{17}$$

To limit each phase current in the allowable range at any electric angles, the maximum value of the current limitation I_m should be adopted as the current constraint. The current limitation function in (17) can be plotted in the form of per unit related to i_q, as shown in Fig. 7.

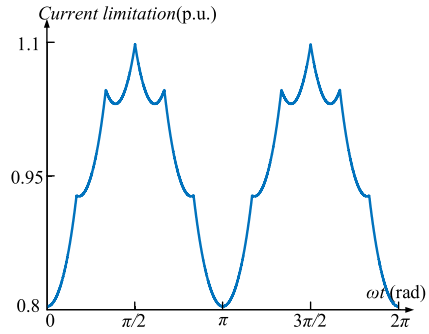

Fig. 7. Current limitation for open-winding DTP-PMSM drives in LSFO.

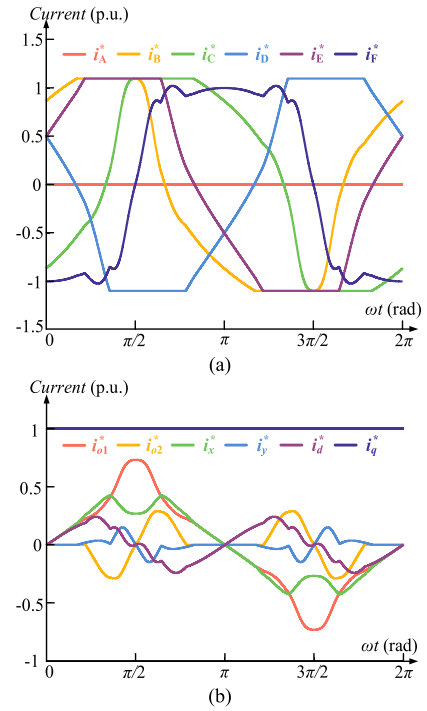

Fig. 8. Current references of the proposed maximum-torque optimization control scheme of open-winding DTP-PMSM drives in LSFO. (a) Six-phase currents. (b) Currents on d–q, x–y, and o_1–o_2 subspaces.

It can be seen from Fig. 7 that the current limit will reach the maximum value of 1.098 at the electric angle of $\pi/2$ and $3\pi/2$. Thus, each phase current must remain within the range denoted by the inequality constraint $-1.098 \le i_X \le 1.098$, where i_X represents the phase-X current. Taking phase-A open-circuit fault as an example, the optimization problem of MTOC problem for LFSO can be expressed in (18) by combining the objective function of copper loss in (5) and the current constraint in (7)

$$\begin{aligned} &\min\ P_{\mathrm{Cu}}. \\ &\text{s.t.}\ \begin{cases} g(0, i_B, i_C, i_D, i_E, i_F) = 0 \\ -1.098 \le i_X \le 1.098 \end{cases} \end{aligned} \tag{18}$$

By employing the interior point method at all the discretized electric angles, the phase currents can be plotted in Fig. 8(a), and currents can be transformed into the decoupled current references, as shown in Fig. 8(b). All phase currents satisfy the constraints of calculated limitation, and currents can be expressed by using the same fitting method in Section V-A.

TABLE II
COMPARISON OF COPPER LOSS AND TORQUE OUTPUT CAPABILITY IN MHFO

Fault-tolerant scheme	Maximum RMS phase current (p.u.)	Total copper loss (p.u.)	Torque output capability in MHFO
Healthy operation	1	1	100%
MT Scheme I [29]	1.732	2	57.7%
MT Scheme II [21]	1.512	1.588	66.1%
MT Scheme III [19]	1.364	1.524	73.3%
Proposed MTOC for MHFO	1.215	1.23	82.3%

TABLE III
COMPARISON OF COPPER LOSS AND TORQUE OUTPUT CAPABILITY IN LFSO

Fault-tolerant scheme	Maximum peak phase currents (p.u.)	Total copper loss (p.u.)	Torque output capability in LSFO
Healthy operation	1.414	1	70.7%
MT Scheme I [29]	2.45	2	40.8%
MT Scheme II [21]	2.59	1.588	38.6%
MT Scheme III [19]	2.642	1.524	37.9%
Proposed MTOC for LSFO	1.553	1.267	64.4%

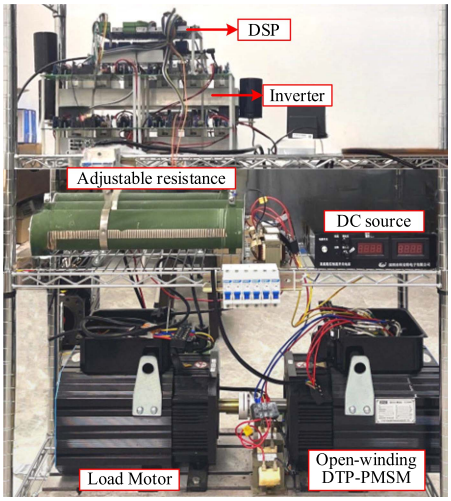

Fig. 9. Experimental platform.

C. Performance Comparison

A comparison is conducted to show the superiority of the proposed MTOC schemes, as given in Tables II and III. Three existing MT fault-tolerant control schemes are compared with the proposed MTOC for MHFO and LFSO, respectively.

Table II gives the comparison of torque output capability and total copper loss in MHFO. Munim et al. [29] utilizes four healthy phases with sinusoidal currents and the torque output capability in MHFO can reach 57.7% with the total copper loss of 2 p.u. By injecting the second harmonics, all five healthy phases are utilized in the shape of nonsinusoidal current waveforms in [21], where the torque output capability is increased to 66.1% and the total copper loss is decreased to 1.588 p.u. Jin et al. [19] optimize the fault-tolerant currents through PSO method with a newly defined objective function. In this way, the torque output loss of 1,524 p.u. The theoretical optimal current references of the proposed MTOC for MHFO are achieved by establishing and solving the quadratic programming problem, and the torque output capability reaches the highest value of 82.3% with a total copper loss of 1.23 p.u.

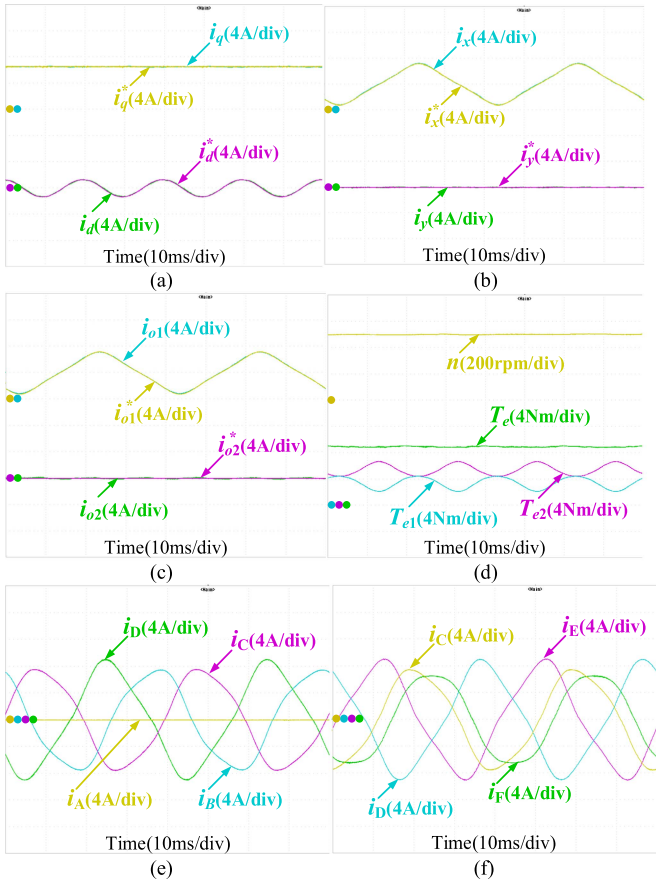

Fig. 10. Proposed MLOC scheme for phase-A open-phase fault of open-winding DTP-PMSM drive, (a) d-axis and q-axis currents, (b) x-axis and y-axis currents. (c) o_1-axis and o_2-axis currents. (d) Speed and torque; (e) Phase-ABCD currents. (f) Phase-CDEF currents.

Table III gives the comparison of torque output capability and total copper loss in LFSO. According to (11), the torque output capability in LFSO is determined by maximum peak value of phase currents which is 1.414 p.u. in healthy operation. Therefore, the torque output capability in LFSO is 70.7%, lower than that in MHFO. Since LFSO is not considered in the existing MT schemes, the proposed MT scheme in LFSO is compared with the three MT schemes in Table II. The torque output capabilities in LSFO of MT schemes in [29], [21], and [19] are 40.8%, 38.6%, 37.9%, respectively. The proposed MTOC for LSFO can improve the torque output capability to the theoretical highest of 64.4% and decrease the total copper loss to 1.267 p.u.

VI. EXPERIMENTAL VERIFICATION

The proposed fault-tolerant optimization control scheme in full operation range is verified on a laboratory prototype of the open-winding DTP-PMSM drive, as shown in Fig. 9. The DSP (TMS320F28337) is adopted to acquire sampling data, execute control strategies, and generate 24 pulsewidth modulation signals. Four sets of three-phase insulated gate bipo-

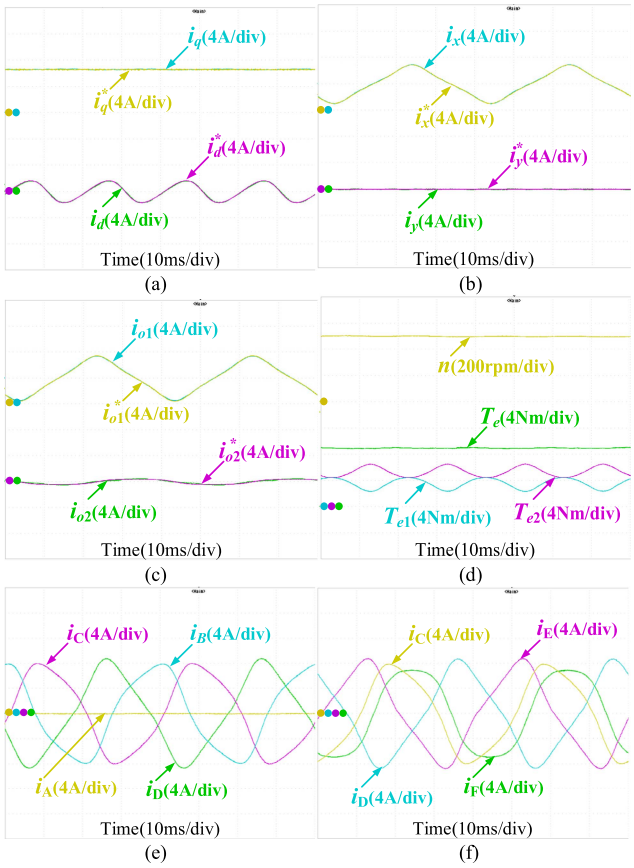

Fig. 11. Proposed MTOC scheme for MHFO with phase-A open-phase fault of open-winding DTP-PMSM drive. (a) d-axis and q-axis currents. (b) x-axis and y-axis currents. (c) o_1-axis and o_2-axis currents. (d) Speed and torque. (e) Phase-ABCD currents. (f) Phase-CDEF currents.

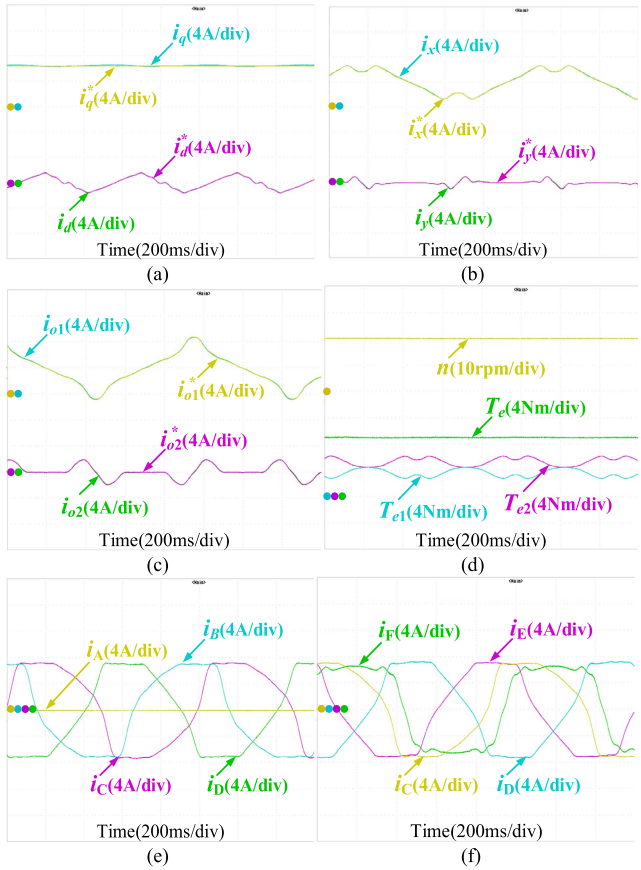

Fig. 12. Proposed MTOC scheme for LFSO with Phase-A open-phase fault of open-winding DTP-PMSM drive. (a) d-axis and q-axis currents. (b) x-axis and y-axis currents. (c) o_1-axis and o_2-axis currents. (d) speed and torque. (e) Phase-ABCD currents. (f) Phase-CDEF currents.

TABLE IV
PARAMETERS OF MOTOR DRIVE

Name	*Value*
Pole pair number	3
d-axis inductance	3.55 mH
q-axis inductance	3.55 mH
PM flux	0.155 Wb
Resistance	0.55 Ω
Given Speed	500 r/min
Load torque	8.8 N.m
Switching frequency	10 kHz

DTP-PMSM. In the experiment, the load torque can be adjusted by changing the load resistance. The open-phase fault is performed by opening the breaker in the faulty phase. The key parameters of the open-winding DTP-PMSM are given in Table IV. To prove the effectiveness of the proposed fault-tolerant control scheme, all the experiments are carried out under phase-A open-phase fault, as shown in Figs. 10 –13.

Fig. 10 shows the experimental fault-tolerant performance of the proposed MLOC scheme with phase-A open-phase fault of open-winding DTP-PMSM drive at the frequency of 25 Hz and the load torque of 8.8N. Fig. 10(a)–(c) depict the tracking performance of decoupled currents which can all track the given corresponding current references. x-axis and o_1-axis currents coincide. Meanwhile, y-axis and o_2-axis currents also coincide. The torque T_e and its distribution of the two three-phase windings T_{e1}, T_{e2} are shown in Fig. 10(d), and the two components jointly produce a steady torque output. Fig. 10(e) and (f) shows the six-phase currents which matched well with the calculated theoretical waveforms in Fig. 5(a).

Fig. 11 shows the experimental fault-tolerant performance of the proposed MTOC scheme for MHFO with Phase-A open-phase fault of open-winding DTP-PMSM drive at the frequency of 25 Hz and the load torque of 8.8 N. Fig. 11(a)–(c) depicts the tracking performance of decoupled currents which can all track the given corresponding current references. The torque T_e and its distribution of the two three-phase windings T_{e1}, T_{e2} are shown in Fig. 11(d), and the two components together produce a steady torque output. Fig. 11(e) and (f) shows the six-phase currents which matched well with the calculated theoretical waveforms in Fig. 6(a). The current of phase-D and phase-E are relatively smaller than that in Fig. 10(e) and (f). This occurs because the objective function of MTOC for MHFO is to minimize the maximum phase copper loss whereas that of MLOC is to minimize the total copper loss.

Fig. 12 shows the experimental fault-tolerant performance of the proposed MTOC scheme for LFSO with phase-A open-phase fault of open-winding DTP-PMSM drive at the frequency of

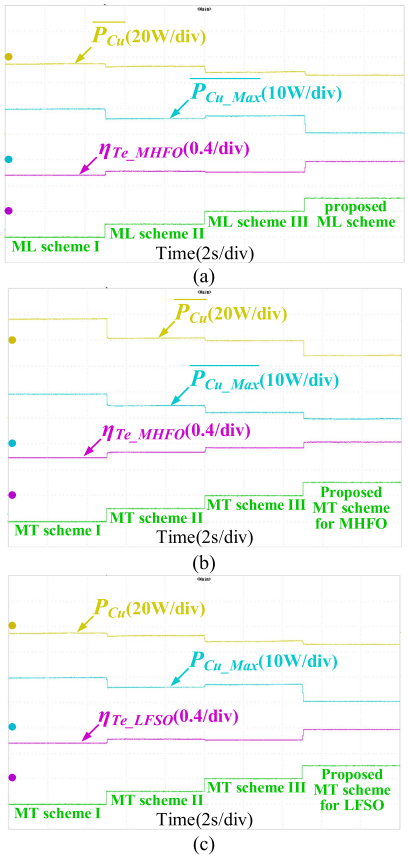

Fig. 13. Performance comparison of different control schemes with phase-A open-phase fault in full operation range. (a) ML schemes. (b) MT schemes for MHFO. (c) MT schemes for LFSO.

1 Hz. To optimally present the experimental effect in LFSO, the motor is replaced with resistance-inductance loads in experimental platform. The resistance and inductance are set to 0.55 Ω and 2 mH, respectively. Fig. 12(a)–(c) depicts the tracking performance of decoupled currents which can all track the given corresponding current references. The torque T_e and its distribution of the two three-phase windings T_{e1}, T_{e2} are shown in Fig. 12(d), and the two components together produce a steady torque output. Due to constraints of phase currents in (17), the torque output of healthy three-phase windings will be reduced on its peak. Fig. 12(e) and (f) shows the six-phase currents which matched well with the calculated theoretical waveforms in Fig. 8(a). The phase currents can be limited within the given amplitude to maximize the torque output capability in LFSO, which validates the effectiveness of the proposed MTOC for LFSO scheme.

Fig. 13 presents the experimental comparisons of copper losses and torque output capabilities among different fault-tolerant schemes in full operation range. In Fig. 13(a), the average copper losses and torque output capabilities are compared among four ML fault-tolerant schemes in Table I at the frequency of 25 Hz. It can be found that the proposed MLOC scheme outperforms other three ML schemes with reduced copper loss and enhanced torque output capability. In Fig. 13(b), the average copper loss and torque output capability are compared among four MT fault-tolerant schemes in Table II at the frequency of 25 Hz. It can be found that the proposed MTOC scheme for MHFO has the highest torque output capability and lowest average total copper loss. In Fig. 13(c), the real-time copper loss and torque output capability in LFSO are compared among four MT fault-tolerant schemes in Table III at the frequency of 1 Hz. It can be observed that the maximum instantaneous phase copper loss $P_{\mathrm{Cu\_Max}}$ in the conventional MT schemes will be increased, thereby decreasing the torque output capability in LFSO. By comparison, the proposed MTOC scheme for LFSO possesses the highest torque output capability with the lowest copper loss.

VII. Conclusion

This article proposed a fault-tolerant optimization control scheme considering the full operation range for open-winding DTP-PMSM drives under open-phase fault. The characteristics of operation states including torque and frequency are analyzed. MLOC and MTOC problems are established for objectives of minimum copper loss and maximum torque, respectively. The proposed MLOC scheme can be applied in full frequency operation range, while the proposed MTOC scheme considers different operating frequencies separately. Theoretically, the proposed fault-tolerant control scheme can reduce copper loss by 5.2% compared to existing optimal ML schemes, and improve the torque output capability by 9%, 23.6% compared to existing optimal MT schemes in MHFO and LFSO, respectively.

References

[1] E. Levi, F. Barrero, and M. J. Duran, "Multiphase machines and drives - revisited," *IEEE Trans. Ind. Electron.*, vol. 63, no. 1, pp. 429–432, Jan. 2016.

[2] L. Jin, Y. Mao, X. Wang, L. Lu, and Z. Wang, "A model-based and data-driven integrated temperature estimation method for PMSM," *IEEE Trans. Power Electron.*, vol. 39, no. 7, pp. 8553–8561, Jul. 2024.

[3] J. Shen, X. Wang, D. Xiao, Z. Wang, Y. Mao, and M. He, "Online switching strategy between dual three-phase PMSM and open-winding PMSM," *IEEE Trans. Transport. Electrific.*, vol. 10, no. 1, pp. 1519–1529, Mar. 2024.

[4] E. Levi, I. Satiawan, N. Bodo, and M. Jones, "A space-vector modulation scheme for Multilevel open-end winding five-phase drives," *IEEE Trans. Energy Convers.*, vol. 27, no. 1, pp. 1–10, Mar. 2012.

[5] Y. Chen, X. Wang, D. Xiao, D. Ma, X. Yang, and Z. Wang, "Model predictive control of five-level open-end winding PMSM drives," *IEEE Trans. Transport. Electrific.*, to be published, doi: 10.1109/TTE.2024.3382029.

[6] X. Wang, S. Ren, D. Xiao, X. Meng, G. Fang, and Z. Wang, "Fault-tolerant control of open-circuit faults in standard PMSM drives considering torque ripple and copper loss," *IEEE Trans. Transport. Electrific.*, vol. 10, no. 2, pp. 4239–4251, Jun. 2024.

[7] P. F. C. Goncalves, S. M. A. Cruz, and A. M. S. Mendes, "Online diagnostic method for the detection of high-resistance connections and open-phase faults in six-phase PMSM drives," *IEEE Trans. Ind. Appl.*, vol. 58, no. 1, pp. 345–355, Jan./Feb. 2022.

[8] K. Yu, Z. Wang, M. Gu, and X. Wang, "Universal control scheme of dual three-phase PMSM drives with single open-phase fault," *IEEE Trans. Power Electron.*, vol. 37, no. 12, pp. 14034–14039, Dec. 2022.

[9] J. Hang, S. Ding, J. Zhang, M. Cheng, and Q. Wang, "Open-phase fault detection in delta-connected PMSM drive systems," *IEEE Trans. Power Electron.*, vol. 33, no. 8, pp. 6456–6460, Aug. 2018.

[10] L. Jin, X. Wang, Y. Mao, L. Lu, and Z. Wang, "Online attribute matching based few-sample data-driven diagnosis of electrical faults in PMSM drive," *IEEE Trans. Power Electron.*, vol. 39, no. 2, pp. 2620–2631, Feb. 2024.

[11] Z. Zhang, X. Wang, D. Xiao, Y. Zhou, M. He, and Z. Wang, "A novel 3-D space vector modulation strategy for open-end winding PMSM," *IEEE Trans. Ind. Electron.*, vol. 71, no. 8, pp. 8536–8547, Aug. 2024.

[12] M. J. Duran and F. Barrero, "Recent advances in the design, modeling, and control of multiphase machines—Part II," *IEEE Trans. Ind. Electron.*, vol. 63, no. 1, pp. 459–468, Jan. 2016.

[13] F. Jen-Ren and T. A. Lipo, "Disturbance-free operation of a multiphase current-regulated motor drive with an opened phase," *IEEE Trans. Ind. Appl.*, vol. 30, no. 5, pp. 1267–1274, Sep./Oct. 1994.
[14] S. Dwari and L. Parsa, "An optimal control technique for multiphase PM machines under open-circuit faults," *IEEE Trans. Ind. Electron.*, vol. 55, no. 5, pp. 1988–1995, May 2008.
[15] H. S. Che, M. J. Duran, E. Levi, M. Jones, W. P. Hew, and N. A. Rahim, "Postfault operation of an asymmetrical six-phase induction machine with single and two isolated neutral points," *IEEE Trans. Power Electron.*, vol. 29, no. 10, pp. 5406–5416, Oct. 2014.
[16] X. Wang, Z. Wang, M. He, Q. Zhou, X. Liu, and X. Meng, "Fault-tolerant control of dual three-phase PMSM drives with minimized copper loss," *IEEE Trans. Power Electron.*, vol. 36, no. 11, pp. 12938–12953, Nov. 2021.
[17] W. Wang, J. Zhang, M. Cheng, and S. Li, "Fault-tolerant control of dual three-phase permanent-magnet synchronous machine drives under open-phase faults," *IEEE Trans. Power Electron.*, vol. 32, no. 3, pp. 2052–2063, Mar. 2017.
[18] G. Feng, C. Lai, W. Li, Y. Han, and N. C. Kar, "Computation-efficient solution to Open-phase fault tolerant control of dual three-phase interior PMSMs with maximized torque and minimized ripple," *IEEE Trans. Power Electron.*, vol. 36, no. 4, pp. 4488–4499, Apr. 2021.
[19] L. Jin, Y. Mao, X. Wang, P. Shi, L. Lu, and Z. Wang, "Optimization-based maximum-torque fault-tolerant control of Dual three-phase PMSM drives under open-phase fault," *IEEE Trans. Power Electron.*, vol. 38, no. 3, pp. 3653–3663, Mar. 2023.
[20] F. Baneira, J. Doval-Gandoy, A. G. Yepes, O. Lopez, and D. Perez-Estevez, "Control strategy for multiphase drives with minimum losses in the full torque operation range under single open-phase fault," *IEEE Trans. Power Electron.*, vol. 32, no. 8, pp. 6275–6285, Aug. 2017.
[21] J. Sun, Z. Liu, Z. Zheng, and Y. Li, "An online global fault-tolerant control strategy for symmetrical multiphase machines with minimum losses in full torque production range," *IEEE Trans. Power Electron.*, vol. 35, no. 3, pp. 2819–2830, Mar. 2020.
[22] Y. Hu, Y. Feng, and X. Li, "Fault-tolerant hybrid current control of dual three-phase PMSM with one phase open," *IEEE J. Emerg. Sel. Topics Power Electron.*, vol. 10, no. 3, pp. 3418–3426, Jun. 2022.
[23] Y. Zhao and T. A. Lipo, "Space vector PWM control of dual three-phase induction machine using vector space decomposition," *IEEE Trans. Ind. Appl.*, vol. 31, no. 5, pp. 1100–1109, Sep./Oct. 1995.
[24] Y. Zhang, H. Wang, Z. Wang, Y. Yang, and F. Blaabjerg, "A simplification method for power device thermal modeling with quantitative error analysis," *IEEE J. Emerg. Sel. Topics Power Electron.*, vol. 7, no. 3, pp. 1649–1658, Sep. 2019.
[25] S. J. Kim, K. Koh, M. Lustig, S. Boyd, and D. Gorinevsky, "An interior-point method for large-scale $\ell 1$-regularized least squares," *IEEE J. Sel. Topics Signal Process.*, vol. 1, no. 4, pp. 606–617, Dec. 2007.
[26] M. Tousizadeh, H. S. Che, J. Selvaraj, N. A. Rahim, and B. T. Ooi, "Performance comparison of fault-tolerant three-phase induction motor drives considering current and voltage limits," *IEEE Trans. Ind. Electron.*, vol. 66, no. 4, pp. 2639–2648, Apr. 2019.
[27] L. Lu, Y. Mao, X. Wang, L. Jin, and Z. Wang, "Maximum-torque optimization control of dual three-phase PMSM in low-frequency and static operations," *IEEE J. Emerg. Sel. Topics Power Electron.*, vol. 11, no. 5, pp. 5268–5278, Oct. 2023.
[28] I. Gonzalez-Prieto, M. J. Duran, and F. J. Barrero, "Fault-tolerant control of six-phase induction motor drives with variable current injection," *IEEE Trans. Power Electron.*, no. 10, Oct. 2017.
[29] W. N. W. A. Munim, M. J. Duran, H. S. Che, M. Bermúdez, I. González-Prieto, and N. A. Rahim, "A unified analysis of the fault tolerance capability in six-phase induction motor drives," *IEEE Trans. Power Electron.*, vol. 32, no. 10, pp. 7824–7836, Oct. 2017.

Linlin Lu (Student Member, IEEE) received the B.S. degree in communication engineering from Zhengzhou University, Zhengzhou, China, in 2021. She is currently working toward the Ph.D. degree in measuring technology and instrument with the Institute of Optics and Electronics, Chinese Academy of Science, Beijing, China.

Her current research interests include the loss optimization and tolerant control of multiphase and open-winding motor drives.

Xueqing Wang (Senior Member, IEEE) received the B.S. degree in electrical engineering from Tianjin University of Science and Technology, Tianjin, China, in 2014, and the M.S. and Ph.D. degrees from Southeast University, Nanjing, China, in 2016 and 2020, respectively, both in electrical engineering.

From 2018 to 2019, he was a joint Ph.D. with McMaster Automotive Resource Centre, McMaster University, Hamilton, ON, Canada. He is currently an Associate Research Fellow with the College of Electrical Engineering, Sichuan University, Chengdu, China. His research interests include control of multiphase motor and open-winding motor, fault diagnosis and tolerant control of motor drive, multilevel PWM strategy.

Luhan Jin (Student Member, IEEE) received the B.S. degree in communication engineering from Zhengzhou university, Zhengzhou, China, in 2021. He is currently working toward the Ph.D. degree in measuring technology and instrument with the Institute of Optics and Electronics, Chinese Academy of Science, Beijing, China.

His current research interests include the fault diagnosis and tolerant control of motor drives and distributed multi-agent system, digital twin modeling and control optimization of motor drives.

Yao Mao (Member, IEEE) received the B.S. degree in automatic control from the Department of Automation, Chongqing University, Chongqing, China, in 2001, and the Ph.D. degree in signal and information processing from the Institute of Optics and Electronics, Chinese Academy of Science, Beijing, China, in 2012.

He has been a Professor with the University of Chinese Academy of Sciences since 2016. His research interests include power electronics, motion control, information fusion, machine learning.

Dr. Mao was the recipient of Distinguished Scientific Achievement Award by the Chinese Academy of Science in 2011.

Qiliang Bao (Member, IEEE) received the B.S. degree in control engineering from Northwestern Polytechnical University, Xi'an, China, in 1989, and the M.A. degree in optoelectronic engineering from the University of Electronic Science and Technology of China, Chengdu, China, in 2004.

He is currently a Researcher with the Institute of Optics and Electronics, Chinese Academy of Sciences, Chengdu, China. His research interests include deep learning and beam control.

Zheng Wang (Senior Member, IEEE) received the B.Eng. and M.Eng. degrees from Southeast University, Nanjing, China, in 2000 and 2003, respectively, and the Ph.D. degree from The Uxniversity of Hong Kong, Hong Kong, in 2008, all in electrical engineering.

From 2008 to 2009, he was a Postdoctoral Fellow in Ryerson University, Toronto, ON, Canada. He is currently a Full Professor with the School of Electrical Engineering, Southeast University, Nanjing, China. He has authored or coauthored more than 80 internationally refereed papers and four books in these areas. His research interests include electric drives, power electronics, and distributed generation.

Dr. Wang received several academic awards including IEEE PES Chapter Outstanding Engineer Award and Best Paper Award of International Conference on Electrical Machines and Systems.